

The extremely young open cluster NGC 6611

Luminosity function and star formation history

A.N. Belikov¹, N.V. Kharchenko², A.E. Piskunov¹, and E. Schilbach³

¹ Institute of Astronomy of the Russian Academy of Sciences, 48 Pyatnitskaya street, Moscow 109017, Russia (abelikov@inasan.rssi.ru; piskunov@inasan.rssi.ru)

² Main Astronomical Observatory, Golosiiv, 252127 Kiev, Ukraine (nkhar@mao.kiev.ua)

³ Astrophysikalisches Institut Potsdam, An der Sternwarte 16, 14482 Potsdam, Germany (eschilbach@aip.de)

Received 4 June 1999 / Accepted 29 November 1999

Abstract. The stellar content of the young open cluster NGC 6611 was studied on the basis of the data of the Compiled Catalogue published in Belikov et al. (1999b). Using photometric and proper motion criteria as well as taking into account the cluster structure, we selected 376 probable members down to $M_V \approx 3^m$ (a limit never reached before) from 2185 catalogue stars. The observed luminosity function was constructed and compared with the theoretical luminosity function computed with the log-normal and power-law IMFs and under the assumption of a non-coeval star formation. From this comparison, the following main conclusions can be drawn, also supported by the analysis of the cluster color-magnitude diagram: (1) the expected H-feature due to the Pre-Main-Sequence – Main-Sequence transition is marginally present in the observed luminosity function at $M_V \approx 1^m$ (i.e., at the supposed turn-on point of the cluster’s CMD); (2) in the mass range $[2.1, 85] m_\odot$ the mass function of cluster stars could be better represented by a power-law IMF with a logarithmic slope $\Gamma = -1.2$ than by a log-normal IMF; (3) a cluster age of 6 Myr derived both from the LF and CMD analysis coincides well with present-day findings. A considerable (of the order of the cluster age) spread of individual ages of cluster stars was confirmed, but no evidence of a sequential star formation was found from the data.

Key words: Galaxy: open clusters and associations: individual: NGC 6611 – stars: luminosity function, mass function – stars: pre-main sequence

1. Introduction

For the last two decades, the young open cluster NGC 6611 has attracted the attention of different researchers. Its large distance, heavy obscuration, rich stellar fore- and background, however, make the observations of this cluster extremely difficult. The first photometric study of NGC 6611 was carried out by Walker (1961) who found massive stars in the cluster color-magnitude diagram (CMD) above the Main Sequence (MS). During the following years, several photometric, spectroscopic,

and proper motion surveys (e.g., van Schewick 1962, Kamp 1974, Sagar & Joshi 1979, Tucholke et al. 1986, Thé et al. 1990, Hillenbrand et al. 1993, de Winter et al. 1997) were obtained in this region. The data enabled careful investigations of the brightest population of the cluster, especially, the construction of its luminosity function (LF) and CMD which were used for study of star formation in the cluster. The comparison of Hertzsprung-Russell diagram of the cluster with theoretical models showed that not one single age could be assigned for the whole cluster. The cluster age corresponding to the “oldest” cluster members was determined to be about 5 Myr (see e.g., Hillenbrand et al. 1993, Massey et al. 1995, and de Winter et al. 1997).

Since NGC 6611 is richly populated by early-type stars, the luminosity or mass functions of this cluster can tell us much on the initial mass function (IMF) of the galactic disk stars. In this respect, NGC 6611 seems to be a very peculiar cluster. For the first time, an extremely flat luminosity function of the NGC 6611 stars was derived by Sagar & Joshi (1979). Comparing the cluster CMD with stellar models, Sagar et al. (1986) found that the logarithmic slope Γ of the cluster mass function (MF) within the range $8 \div 70 m_\odot$ is about $-0.8 \div -0.9$. A similar value ($\Gamma = -0.7$) for the same mass range was also determined by Massey et al. (1995) for NGC 6611. However, based on the same data but a slightly different mass calibration, Hillenbrand et al. (1993) found $\Gamma = -1.1 \div -1.3$.

From these results, the question arises whether the IMF flattening with decreasing galactocentric distance is a real property of the disk population or if it is rather an artifact coming from the incompleteness of the data due to the large distance of the cluster and its heavy visual obscuration. Since NGC 6611 is one of a few young distant clusters observed towards the Galactic Center, each effort to improve the data base for NGC 6611 can make an important contribution by answering this fundamental question.

An additional reason for our special interest in this cluster can be described as following. As it was found in the previous theoretical investigations by Piskunov & Belikov (1996), the presence of Pre-Main-Sequence (Pre-MS) stars in a cluster affects its luminosity function by producing an additional detail (we call it H-feature) in its LF. The H-feature reveals as a

local inhomogeneity in a cluster LF consisting of a bump with a trailing depletion. The H-feature results from a non-uniform behaviour of the mass-luminosity relation in the vicinity of the turn-on point of a cluster's HRD. Since the location of the H-feature on the absolute magnitude axis depends on cluster age, LFs of young clusters can be used for independent age estimation (H-calibration according to Belikov & Piskunov 1997). This feature was found in the luminosity functions published for several young clusters (Belikov & Piskunov 1997) as well as in the Pleiades LF (Belikov et al. 1998, Belikov et al. 1999a). In contrast to the Pleiades, NGC 6611 belongs to the youngest end of the H-calibration. According to the results of the H-calibration, the H-detail should occur at $M_V = 0^m \div 2^m$ for a 5 Myr old cluster. Due to the large distance of NGC 6611 (with distance modulus being $V - M_V \approx 14^m$), the data available so far were not sufficiently complete to construct a reliable luminosity function down to this limit. The situation was improved with the Compiled Catalogue of photometric and astrometric data in the field of NGC 6611 (Belikov et al. 1999b, Paper I hereafter).

The Compiled Catalogue (CC hereafter) covers a circular area with a diameter of 45.6 arcmin which is centered at the NGC 6611 cluster. The survey contains astrometric (positions, absolute proper motions) and photometric (photoelectric, CCD, and photographic UBV magnitudes as well as color excesses) data for 2185 stars brighter than $V = 16.8^m$. The catalogue is based on the Tautenburg Schmidt survey supplemented by the relevant data published in this region which were reduced to a common homogeneous system.

Since the CC has a completeness limit which should allow to reach the H-feature in the LF of NGC 6611, the present study is aiming at the following major goals. First, the construction of a confident and deep luminosity function of cluster stars based on a careful analysis of proper motion and photometric membership, as well as by taking into account the cluster structure and distribution of absorption across the cluster. Secondly, the comparison of the empirical and theoretical LFs by considering different assumptions on star formation history of the cluster. Third, the determination of the cluster parameters describing this process i.e., onset and duration of star formation, cluster age, and MF slope.

In Sect. 2 the results on the cluster's structure and stellar content based on the the CC data are presented. In Sect. 3 we use these results for a better selection of cluster members yielding a sample down to $M_V \approx 3^m$. Sect. 4 describes how the empirical and theoretical luminosity function were constructed for the NGC 6611 cluster. In Sect. 5 we compare these LFs and discuss the results on star formation history of the cluster. The conclusions from this study are presented in Sect. 6.

2. Compiled catalogue: Cluster structure and stellar content

In Fig. 1 we show the X, Y -plane of NGC 6611 with stars from the CC and the main structure elements of the cluster (the core and corona) as derived in Paper I. In order to get an idea on

the patchy distribution of interstellar matter across the cluster surface, we also plotted the isophote outlining the H_β emission nebulosity as seen on a blue NGPOSS plate (taken from Kamp 1974) and the absorption distribution A_V according to the absorption map given in Paper I.

The A_V -values displayed in Fig. 1 by grey color were determined from individual data on reddening E_{B-V} and total-to-selective absorption ratio R_V as described in Paper I. For stars in outer parts of the cluster region, no data are available for individual correction of magnitudes due to the absorption. In the following, for these stars we adopted the averaged values $E_{B-V} = 0.86^m$ and $R_V = 3.75$ estimated by Hillenbrand et al. (1993) for this cluster. This approach could lead to incorrect results in studies of properties of a particular star with an unknown individual extinction law. In the case of statistical investigations of stellar samples (such as the determination of luminosity or mass functions), we can expect, however, that a statistical bias introduced by the averaged reddening values will be of a considerably less significance. We tested various approaches for the treatment of the extinction law (e.g., the normal extinction with $R = 3.1$, the interpolation of the absorption map, the extinction parameters of the nearest neighbour and the interpolation between the individual values of the nearest neighbours), and we found that the resulting cluster parameters were robust to the extinction laws used, i.e. they either varied within estimated accuracy or did not change at all.

In Fig. 2 the radial density profiles of the distribution of stars from the CC are shown. There is a steady decrease of the total stellar density up to $\approx 14 \text{ arcmin}$ (Fig. 2a) that is close to the edge of the cluster corona $r_c = 3 \sigma_{XY}^{\text{corona}} = 14.3 \text{ arcmin}$ estimated in Paper I. Assuming the density of field stars to be the minimum density over the area covered the CC, we may conclude that at $r > r_c$ no cluster members are virtually present, whereas in the corona there is a mixture of cluster and field stars (from the density relation between the outer region and corona, we can deduce that the contamination of the corona by field stars is more than 80%).

In general, the distribution of CC stars reveals a central symmetry. However, small differences can be seen between the profiles in different azimuthal sections (panels from 2b to 2g). The difference is most prominent between two cluster areas, the "North-West" (NW) and "South-East" (SE) areas (dashed and dotted curves in Fig. 2a), separated by a line

$$Y = 0.571 X + 1.012$$

This can be attributed rather to local irregularities of the absorption distribution (cf. Fig. 1) than to a real lack of stars in the NW part of the corona. In the outer areas of the NW corona, the stellar density is lower than in a surrounding field (especially, in the sector $90^\circ \div 210^\circ$). It appears as if the cluster is still embedded in the interstellar dust in its NW part, whereas in the SE part the cluster is already cleared off by a bubble of the hot gas expanding from the center.

Assuming that 1) the majority of stars observed in the core belongs to the cluster, 2) the sample of stars projected on the corona presents a mixture of cluster members and field stars, and

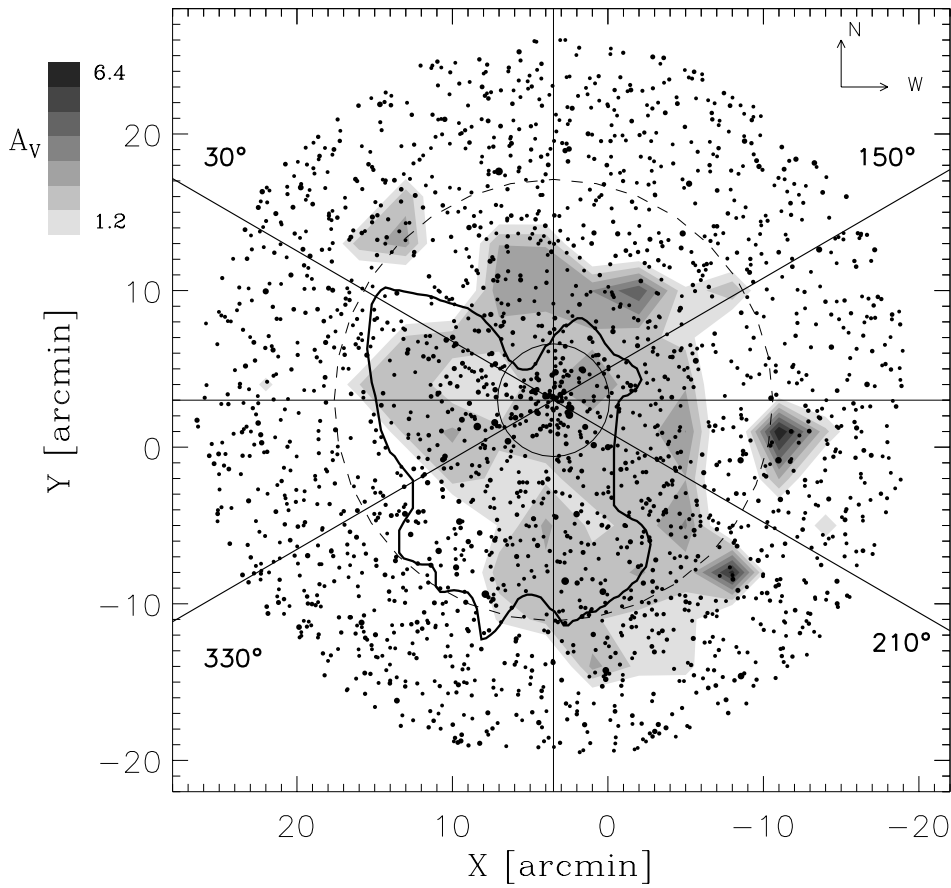


Fig. 1. Distribution of the CC stars in the NGC 6611 region. The coordinates are given with respect to Walker's star 125 (α, δ)_{2000.0} = $18^h 18^m 26.21^s, -13^\circ 50' 05.3''$. The lines divide the cluster area into azimuthal sectors denoted by the corresponding numbers. The thick solid curve marks the isophote of the bright nebula M 16 taken from Kamp (1974). A small circle (thin continuous curve) indicates the cluster core, whereas the cluster edge ($3\sigma_{corona}$) is shown by a large circle (thin dashed line). The distribution of absorption A_V as derived in Paper I is illustrated by a grey-scaled color according to the scale plotted in the upper left corner. Areas where no individual data on absorption are available are indicated by white color.

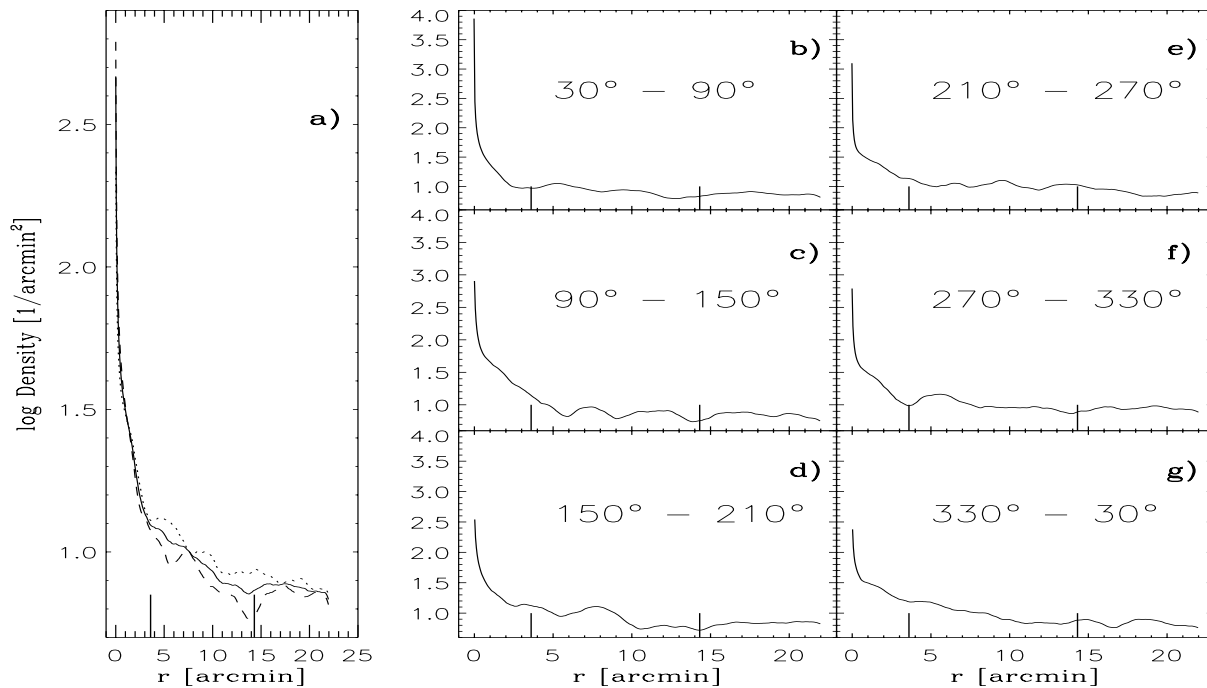


Fig. 2a – g. Radial density profiles over the cluster area. Panel **a** shows the density profile for all CC stars (solid line), for the NW segment $30^\circ \div 210^\circ$ (dashed line) and for the SE segment $210^\circ \div 30^\circ$ (dotted line). Panels **b** through **g** show the density distribution in each sector. The derived size of the cluster core and corona are marked on the abscissa by small vertical lines. All curves are normalized to the number of the CC stars.

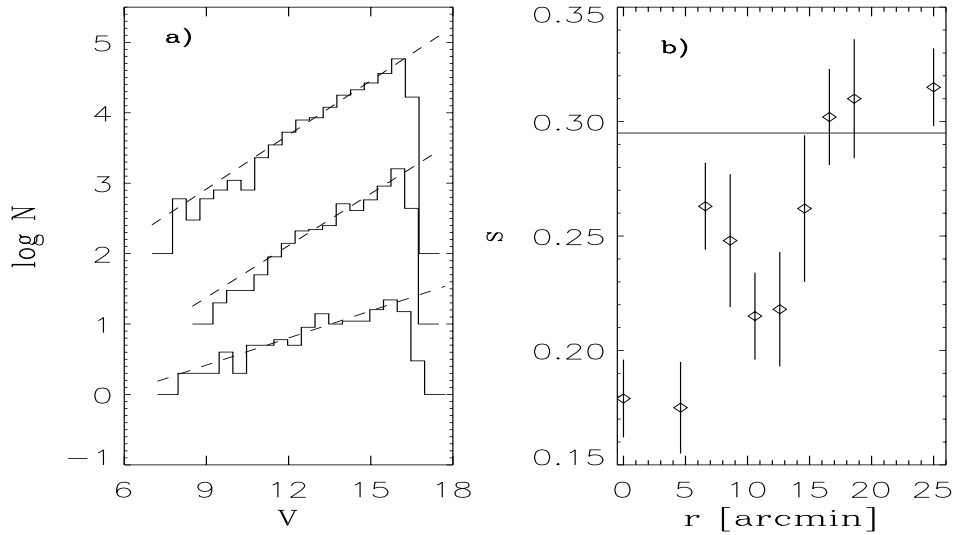


Fig. 3a and b. Histograms of brightness distribution (Panel a) are plotted for all stars from the CC (top), for the outermost area $r > 19.6 \text{ arcmin}$ (middle), and for the cluster core $r < 3.6 \text{ arcmin}$ (bottom). For an easier comparison, the histograms are arbitrary shifted along the ordinate and approximated by lines. The corresponding slopes s of the BFs are given in Panel b as function of radial distance from cluster center. The slope of the brightness distribution of all catalogue stars is $s = 0.295$; that is indicated by the horizontal line in Panel b.

3) cluster members are practically absent outside the corona, we may expect to see variations in the distribution of stars with apparent magnitude as a function of angular distance from the cluster centre.

The brightness function (BF) based on the CC data i.e., the distribution of the catalogue stars with apparent V magnitude, is shown in Fig. 3a. From the comparison of the BFs for the core and outermost areas covered by the CC, we can conclude that the slope of the core BF differs drastically from the slope of the outer BF which in turn is close to the slope of the BF of all stars included in the CC. In Fig. 3b we show slopes of the BFs derived in concentric rings around the cluster center. According to this plot, we can again discriminate three different groups of stars: the core population dominated by cluster members, the corona population consisting of cluster and field stars, and the “external” population (stars outside the corona border) which is practically free of cluster members.

The following conclusions could be drawn from the first look on the CC data:

- the cluster structure consisting of two components (core and corona) as proposed in Paper I is supported by the population analysis;
- the distribution of the visual absorption in the cluster corona is highly inhomogeneous. In spite of general radial symmetry found for the cluster, there is some lack of stars as counted in the NW part of the cluster area;
- most of the stars in the CC are field stars, but their fraction is decreasing from the outer areas to the cluster center.

Based on these results, we can conclude that besides the usual methods, additional efforts are required for a proper selection of cluster members in NGC 6611.

3. Field star de-contamination

Usually, the distribution of proper motions is considered as a good astrometric criterion for selection of cluster members. However, for distant clusters, the individual proper motions of

their members are rather small and differ insignificantly from the proper motions of field stars. In other words, due to numerous field stars with $\mu_{field} \approx \mu_{cluster}$ in the cluster area, the number of cluster members estimated from the proper motion distribution is never zero at any distance from the cluster center. Therefore, additional and independent criteria are needed for a confident selection of cluster members.

In Paper I we considered the distribution of star positions as a further selection criterion and determined the formal membership probability for each CC star. This method, however, requires predefined parameters of the cluster structure (e.g., cluster radius). Insufficiently accurate input parameters may introduce biases both in the computed membership and in the final cluster size. A further possibility is to use photometric criteria i.e., to analyse the loci of cluster candidates in the CMD. This approach allows, with a certain confidence, to reject stars falling below the cluster MS. Finally, as a selection criterion, one can consider the distribution of stars as a function of apparent magnitude which, as was shown in the previous section, should be different for field and cluster stars. With different weight, all these criteria were applied in this study to support the proper motion membership.

3.1. De-contamination procedure

Among other data, the CC contains probabilities for stars to belong to the core or corona of NGC 6611. The probabilities were deduced from the distributions of positions and/or proper motions. In the following, we use the probabilities $P(pm, xy, core)$, and $P(pm, xy, corona)$ for the final cluster membership determination.

We divided all CC stars into five groups with respect to their proper motions and positions.

1. The group of 111 stars from Walker’s (1961) list. Due to crowding effects, these stars were not measured on Tautenburg Schmidt plates and, therefore, have no proper motions in the CC. They show a concentration to the cluster center

which is compatible with cluster membership. As a basic criterion, the loci of these stars in the CMD were considered (see Sect. 3.3 for details).

2. Non-members according to the kinematic criterion. These stars belong to a high-velocity wing of the proper motion distribution and are presumably nearby foreground stars. They can be clearly rejected as cluster members at the 3σ -level.
3. Candidates of the cluster core. This poorly populated group of proper motion members shows a strong concentration to the cluster center. Due to the small core size, only a low contamination by field stars projected on the core may be expected. Therefore, these stars can be considered as typical representatives of the cluster population. In order to improve their membership determination, the photometric selection criterion was additionally applied (Sect. 3.3).
4. Candidates of the cluster corona. This group of suspected proper motion members does not show a concentration to the cluster center. According to the conclusions in Sect. 2, this group can include a large fraction of field stars. Therefore, additional tools were necessary to improve the membership determination. For these stars we proposed a “local probability” technique described in Sect. 3.2. As final step, the photometric selection criterion was applied (Sect. 3.3).
5. Non-members. This group includes the remaining CC stars. They have low probabilities to belong to the core and were rejected as corona members by the “local probability” technique, too.

3.2. The local probability method of the selection of cluster members in the corona

As we already discussed above, the stars located outside the cluster core represent a mixture of corona members and field stars. A clear separation of these stars in two groups (i.e., in the groups 4 and 5 as described in the previous section) from their positions and proper motions is rather difficult. Therefore, we applied an additional selection criterion to these stars taking into account specific features of the corona population.

According to Sect. 2, the apparent structure of the corona is highly variable due to irregularities of the absorption over the cluster surface. Therefore, we considered a relation between the absorption and a “threshold” membership probability derived from the proper motion distribution within a given sub-area. Such a relation can be expected for the following reasons. Due to variations of the absorption across the cluster, the real luminosity function of the cluster stars is transformed to an observed brightness function depending also on coordinates. Since the accuracy of proper motions depends on the apparent brightness of stars, the resulting distribution of proper motion errors will also depend on coordinates. Consequently, the threshold membership probability p_0 which is related to the error distribution is also a function of positions. On the other hand, with increasing absorption A_V both numerous faint background stars and faint companions of apparently close pairs (unresolved on photographic plates) are lacking from a survey. The visible pho-

tocentre of such a pair moves towards the bright component and the astrometric accuracy is improving. As the number of stars becomes rapidly small with decreasing magnitude, we may expect, on average, a decrease of the proper motion errors as well of the corresponding threshold membership probability p_0 for stars of a given apparent magnitude in areas with higher A_V .

Based on these considerations and on the difference in the distributions of field and cluster stars with apparent magnitude, we proposed a statistical procedure of the corona members selection. We estimated local membership probabilities by comparing the local BF with the brightness function $\Psi(V)$ of stars from the external CC region ($r > 19.6 \text{ arcmin}$) which is dominated by field stars (cf. Sect. 2). The CC area was divided into 32 small cells with a step of $\Delta r = 6 \text{ arcmin}$, $\Delta\theta = \pi/4$. For stars satisfying the condition $P(pm, xy, corona) < p_0$, we determined the local BF function $\Phi(V, p_0)$ in each cell and compared it with $\Psi(V)$:

$$\chi(p_0) = \sum_V \frac{(\Phi(V, p_0) - \Psi(V))^2}{\Psi(V)}.$$

Function $\chi(p_0)$ reflects the degree of agreement between the field and local BFs for a given p_0 . One can predict the behaviour of $\chi(p_0)$ with increasing p_0 from 0 to 100 per cent. At small p_0 the functions $\Phi(V, p_0)$ and $\Psi(V)$ differ randomly due to a small number of stars selected in a cell. This difference tends to a minimum when p_0 increases up to a certain p_0^a due to the inclusion of new field stars and a decrease of statistical fluctuations. In the vicinity of p_0^a , the value which could be considered as a threshold proper motion probability for the cluster membership, $\chi(p_0)$ starts again to increase due to the admixture of cluster stars.

As an example for the efficiency of the method, we show in Fig. 4 the BFs computed in the cell with $(r, \theta) = (9.0 \text{ arcmin}, 112.5 \text{ deg})$. A threshold probability of $p_0^a = 61\%$ was estimated for this cell. The stars were separated in two groups according to $P(pm, xy, corona) \geq p_0^a$ for cluster members and $P(pm, xy, corona) < p_0^a$ for field stars. From Fig. 4 we can see that the BF derived for field stars in this cell is in excellent agreement with the general field BF, whereas the cluster BF in the cell differs significantly from the field BFs and is in agreement (in its slope) with the core BF shown in Fig. 3. In Table 1 we give the threshold probabilities p_0^a estimated for each cell. As expected, their distribution is strongly correlated with the absorption distribution shown in Fig. 1.

3.3. Photometric selection

Generally, we consider two color-magnitude diagrams ($M_V, (B-V)_0$; $M_B, (U-B)_0$) and a color-color diagram ($(U-B)_0, (B-V)_0$) for a photometric selection (E_{B-V} values were not used as a direct criterion, but they are included implicitly in the photometric selection as a secondary criterion when the reddening-free CMDs were constructed). If no U -magnitude was available in the CC, only the $M_V, (B-V)_0$ diagram was used. Taking into account the magnitude errors given in the CC and the error of the distance modulus (0.1^m in V), we consid-

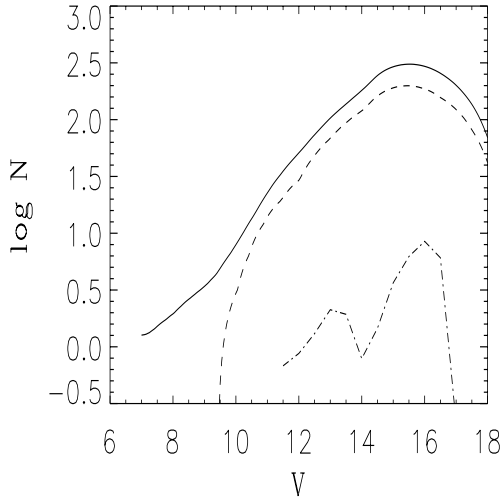


Fig. 4. Membership determination with the local probability method within the area $(r, \theta) = (9.0 \text{ arcmin}, 112.5 \text{ deg})$. The solid curve is the general field BF, the dashed line is the local BF of non-members ($P(pm, xy, corona) < 61\%$) arbitrary shifted along the ordinate for better presentation, and the dotted-dashed line is the BF of corona members ($P(pm, xy, corona) \geq 61\%$).

Table 1. Threshold membership probabilities p_0^a (in%) for the cluster corona

$\theta, \text{ deg}$	radius, arcmin			
	3.0	9.0	15.0	21.0
22.5	20	27	18	17
67.5	82	54	16	10
112.5	15	61	24	7
157.5	78	68	16	10
202.5	61	23	41	10
247.5	33	68	18	14
292.5	64	18	27	16
337.5	18	27	9	13

ered the loci of suspected members in each diagram with respect to the ZAMS by Schmidt-Kaler (1982). A star was rejected as a cluster member if it fell below and to the left of the ZAMS in at least one of the diagrams. In order to derive the reddening-free diagrams, we applied the same procedure and adopted the same parameters as in Paper I: the stars with the available values of E_{B-V} and R_V were dereddened individually, whereas the average values ($E_{B-V} = 0.86^m$, $R_V = 3.75$) were applied otherwise. From a comparison of different approaches of reddening determinations discussed in Sect. 2 we found that these values of the extinction law provide the least fuzzy and most plausible CMDs. The distance modulus $(V_0 - M_V) = 11.65^m$ determined in Paper I from a sample of stars with the most accurate magnitudes and colors was used for the construction of cluster's CMDs.

In Figs. 5,6,7 we show the results of the photometric selection in the membership groups 1, 3 and 4. The final results of the selection are presented in Table 2. The distribution of cluster members in the X, Y -plane is shown in Fig. 8. A non-symmetric

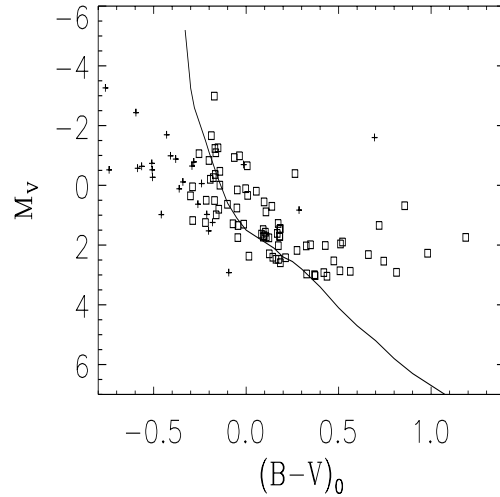


Fig. 5. Color-magnitude diagram of NGC 6611 for suspected members with unknown proper motions (111 Walker's stars, Group 1). The stars accepted as cluster members by the photometric selection are marked by open squares, the rejected – by crosses. The solid curve is the ZAMS according to Schmidt-Kaler (1982).

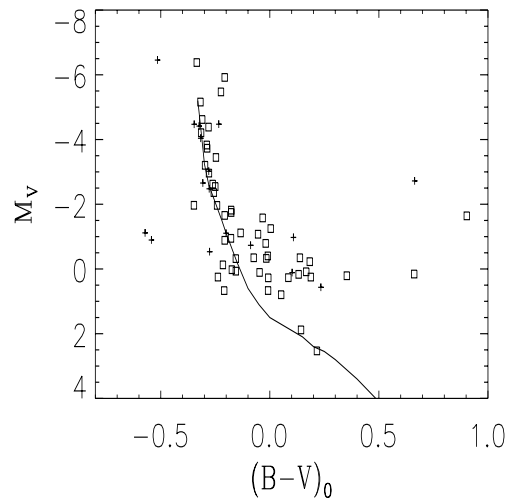


Fig. 6. Color-magnitude diagram of NGC 6611 for suspected core members (Group 3). The stars accepted as cluster members by the photometric selection are marked by open squares, the rejected – by crosses. The solid curve is the ZAMS according to Schmidt-Kaler (1982).

distribution of cluster members over the cluster surface is certainly related to the irregular distribution of the absorbing matter.

The complete catalogue including the astrometric and photometric data as well as membership determination is available in machine-readable form at cdsarc.u-strasbourg.fr (CDS) via anonymous ftp.

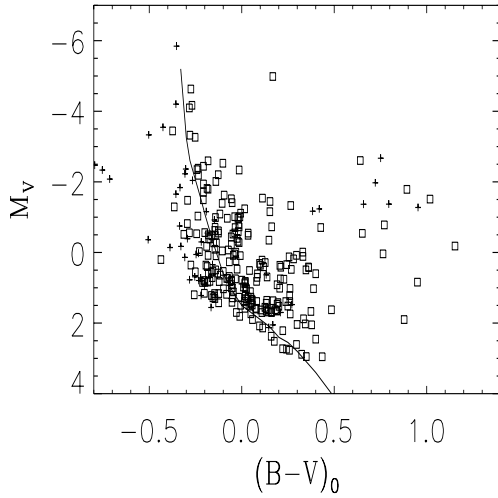
4. Luminosity function

4.1. Construction of the observed LF

In order to reveal details in the LF of NGC 6611, we used a more sophisticated technique than the usual histogram construc-

Table 2. Statistics of the membership determination

No	Membership group	Group indicator	Number of stars	Photomet. rejected	Cluster members
1	“Walker’s stars”	no proper motions are available	111	27	84
2	Kinematic non-members	$P(pm) = 0$	585	–	–
3	Core candidates	$P(pm, xy, core) > 14$	68	17	51
4	Corona candidates	$P(pm, xy, core) \leq 14$ & $P(pm, xy, corona) > p_0^a$	287	46	241
5	Non-members	$P(pm, xy, core) \leq 14$ & $P(pm, xy, corona) \leq p_0^a$	1134	–	–
Total			2185	90	376

**Fig. 7.** Color-magnitude diagram of NGC 6611 for suspected corona members (Group 4). The stars accepted as cluster members by the photometric selection are marked by open squares, the rejected – by crosses. The solid curve is the ZAMS according to Schmidt-Kaler (1982).

tion. A non-parametric smoothing of the distribution was carried out with the kernel density estimation method using the Epanechnikov kernel (see Silverman, 1986 for more details of the method). The luminosity function was computed as

$$\phi_O^*(M_V) = \sum_i K\left(\frac{M_V - M_{Vi}}{h}\right),$$

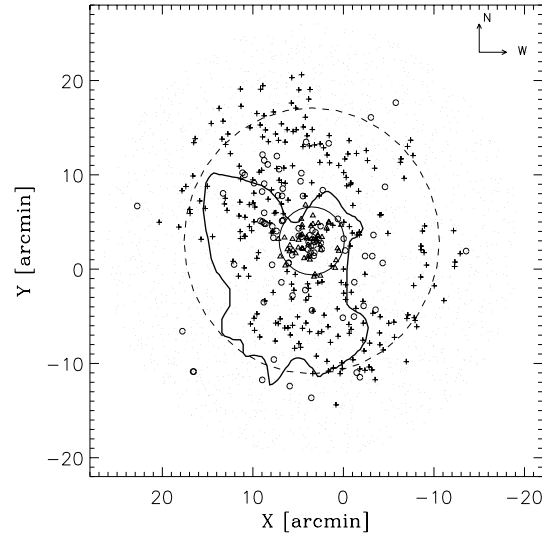
where K is Epanechnikov kernel

$$K(x) = \begin{cases} 3(1 - x^2)/4, & |x| < 1.0 \\ 0, & |x| \geq 1.0 \end{cases}$$

with a smoothing parameter $h = 0.935$ and i running through the data sample. The smoothing parameter was computed by minimizing the mean integrated square errors for the smoothed luminosity function.

4.2. Correction for the incompleteness due to variable absorption

As we already noted above, the distribution of interstellar absorption is highly inhomogeneous in the cluster corona where a typical variation of absorption in the V -band is about 2 or 3

**Fig. 8.** Distribution of cluster members in the X, Y – plane of NGC 6611. Open circles, triangles and crosses indicate the cluster members in group 1, 3 and 4 (according to Table 1), respectively. CC stars not falling into one of the categories above are plotted as dots. The other designations are the same as in Fig. 1.

magnitudes. Therefore, even if the CC is complete down to a given apparent magnitude V^* , the observed luminosity function suffers from the incompleteness within a range of absolute magnitudes $[M_V^1, M_V^0]$:

$$M_V^0 = V^* - (V_0 - M_V) - a_0,$$

$$M_V^1 = V^* - (V_0 - M_V) - a_1,$$

where a_0, a_1 are the minimum and maximum values of the absorption observed in NGC 6611 and $(V_0 - M_V)$ is the true distance modulus. The CC is complete down to M_V^1 and no cluster members with $M_V > M_V^0$ are included in the CC. Below we show how this effect and the corresponding correction to the LF can be evaluated.

Let $\nu(A_V)$ be a distribution function of absorption values for cluster stars

$$\nu(A_V) = \frac{dN}{dA_V}$$

with a normalization

$$\int_{a_0}^{a_1} \nu(a) da = 1.$$

If $\phi(M_V) = dN/dM_V$ is a “true” cluster LF then the number of members we may expect within given ranges of absolute magnitude (M_V , $M_V + dM_V$) and of absorption (a , $a + da$) will be

$$\phi(M_V)\nu(a)dM_V da$$

stars. Integrating this expression over a , we derive an “observed” luminosity function

$$\phi_T^*(M_V) = \phi(M_V) \int_{a_0}^{a^*(M_V)} \nu(a) da = c_a(M_V)\phi(M_V)$$

where, $c_a(M_V)$ is an incompleteness factor, and

$$a^*(M_V) = \begin{cases} a_1, & M_V < M_V^1 \\ V^* - M_V - (V_0 - M_V), & M_V^1 \leq M_V \leq M_V^0 \\ a_0, & M_V > M_V^0. \end{cases}$$

This means that at $M_V < M_V^1$ $c_a = 1$, at $M_V > M_V^0$ $c_a = 0$, and within $[M_V^1, M_V^0]$ c_a varies in accordance with the distribution $\nu(a)$ which is derived from the absorption data in the CC.

From Paper I the maximum spread of the absorption $\Delta a = a_1 - a_0$ reaches almost 7 magnitudes in NGC 6611, while the “half-width” of the absorption distribution is 2.5 magnitudes. In other words, the observed LF will be influenced by this kind of incompleteness at its faint end (at least 2.5 magnitudes). Therefore, we must compare the observations not with the “true” theoretical LF $\phi(M_V)$ but with the “observed” theoretical LF $\phi_T^*(M_V)$.

4.3. Theoretical luminosity function

The “observed” theoretical LF $\phi_T^*(M_V)$ was computed according to

$$\phi_T^*(M_V) = c_a(M_V)\phi(M_V)$$

with

$$\phi(M_V) = \int_{t_0}^{t_1} \phi_t(M_V)\lambda(t) dt,$$

where t_0 and t_1 are minimum and maximum ages of the cluster stars, $\phi_t(M_V)$ is the LF of stars with age t ($t_0 \leq t \leq t_1$), $\lambda(t)$ is the star formation rate (SFR) at age t .

For $\phi_t(M_V)$ we have:

$$\phi_t(M_V) = \left. \frac{dN}{dM_V} \right|_t = f(\log m[M_V, t]) \left| \frac{d \log m}{dM_V} \right|_t$$

where $f(\log m) = dN/d \log m$ is the initial mass function. The mass- M_V relation $m(M_V, t)$ and its derivative were calculated along the isochrone of age t by use of a cubic spline interpolation.

We considered two representations of the IMF:

- a power-law $f(\log m) = km^{-x}$
- a log-normal law $f(\log m) = e^{(c-a \log m - b \log^2 m)}$

where k , x , and a , b , c are parameters.

We assumed a constant SFR for NGC 6611:

$$\lambda(t) = \text{const.}$$

The resulting parameters for NGC 6611 were drawn from the best fit of the theoretical and observed LFs¹.

In order to construct theoretical isochrones and LFs which include both Post-MS and Pre-MS stages for ages typical to that of NGC 6611 (1 to 10 Myr), we combined Population I Pre-MS evolutionary tracks of Palla & Stahler (1993) for model masses from 0.6 to 6 m_\odot , and Maeder’ group Post-MS calculations (Schaller et al., 1992) for $m = 0.8 \div 120 m_\odot$. The grids were properly tuned to provide a continuous transition from Pre- to Post-MS ages at the same mass as well as smooth and uniform mass-luminosity and mass-radius relations along the ZAMS. The models were reduced to the Population I chemical abundance (Y, Z)=(0.30,0.02). The isochrones were computed from the grid of tracks by use of linear interpolation.

In order to convert the theoretical coordinates $\log T_{eff}, \log L/L_\odot$ of the Hertzsprung-Russell Diagram (HRD) to the observed values $(B - V)_0, M_V$, we used bolometric corrections and $(B - V)_0 - \log T_{eff}$ relations from Schmidt-Kaler’s (1982) tables for the luminosity classes I, III and V.

5. Results and discussion

The observed ($\phi_O^*(M_V)$) and fitted theoretical ($\phi_T^*(M_V)$, $\phi(M_V)$) LFs are shown in Fig. 9. The smoothed observed LFs drawn with the solid lines were computed for two sets of data. First, the observed LF (called herewith *restricted* LF) was constructed with stars down to $V^* = 16.4^m$ what corresponds to the completeness limit of the CC estimated in Paper I. The second data set for the LF construction includes all selected members and extends down to the limiting magnitude of the CC (*full* LF). Respectively, the best-fitted theoretical LFs ($\phi_T^*(M_V)$) were computed for the *restricted* and *full* samples which are reproduced by the dotted and dotted-dashed curves in Fig. 9. Additionally, a “true” (incompleteness free) theoretical LF $\phi(M_V)$ based on the same parameters as the *restricted* theoretical LF is drawn with the dashed line.

The “true” theoretical LF $\phi(M_V)$ and “observed” theoretical LF $\phi_T^*(M_V)$ for the *restricted* sample differ only due to the incompleteness factor c_a which was derived from the data on absorption given in the CC. An excellent agreement at faint magnitudes ($0.5^m < M_V < 3^m$) between $\phi_T^*(M_V)$ and the observed *restricted* LF $\phi_O^*(M_V)$ gives an evidence that the observations reflect the H-feature appearing at $M_V > 1^m$ even though the data are not complete at the faint end (see also the discussion below).

In contrast, we consider another detail (a small dip) in the observed LF between $M_V = -4^m$ and $M_V = -2^m$ to be

¹ We also tested a power-law SFR, $\lambda(t) = t^\beta$, and found that the best-fit yielded a β -parameter which did not significantly differ from zero.

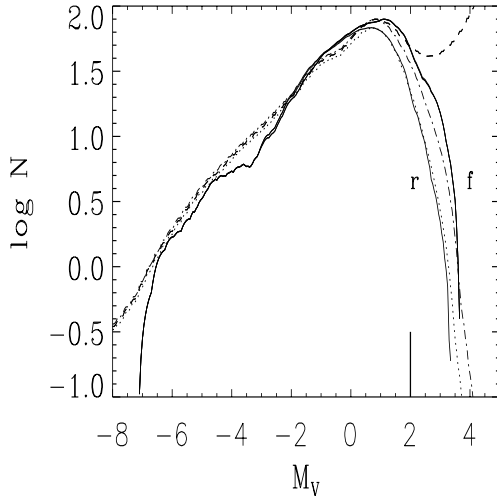


Fig. 9. Comparison of the observed and theoretical luminosity functions. The observed LFs $\phi_O^*(M_V)$ based on the *restricted* (*r*) and *full* (*f*) samples are shown with the solid lines. The corresponding theoretical LFs $\phi_T^*(M_V)$ for the *restricted* and *full* sample are marked by the dotted and dotted-dashed curves, respectively. The theoretical LF $\phi(M_V)$ computed with the parameters from Table 3 without any restrictions for the completeness is drawn with the dashed curve. The vertical bar at $M_V = 2^m$ marks the completeness limit of the *full* sample.

Table 3. NGC 6611 parameters from the LF fitting

Parameter	Value	Note
t_0	1.3	minimum age, Myr
t_1	6.0	maximum age, Myr
$\langle t \rangle$	3.4	average age, Myr
a	3.1	IMF parameter
b	-0.2	IMF parameter
x	1.2	IMF parameter

Note. The parameters were derived for the range of
 – masses: $[2.1, 85] m_\odot$,
 – absolute magnitudes: $[-6.3^m, 2.7^m]$.

caused by statistical fluctuations due to the low number of stars in this magnitude range (see e.g. Fig. 10).

In Table 3 we present the cluster parameters derived from the fit of the *restricted* LF. From the comparison of the results obtained with the *restricted* and *full* samples, we found that the corresponding cluster parameters do not differ significantly. Therefore, we may consider the derived set of the cluster parameters in Table 3 to be unbiased with respect to the incompleteness of the data used. The accuracy of the parameters was evaluated numerically in the vicinity of the minimum of χ^2 -distribution at the 99% significance level. We found that our estimates of the age parameters $t_0, t_1, \langle t \rangle$ are accurate within 25% and the IMF parameters a, b, x have mean errors of about 0.1. It should be stressed that these estimates refer to the accuracy of the fitting method only and do not take into account such important sources of systematic errors as sampling and dereddening errors, inad-

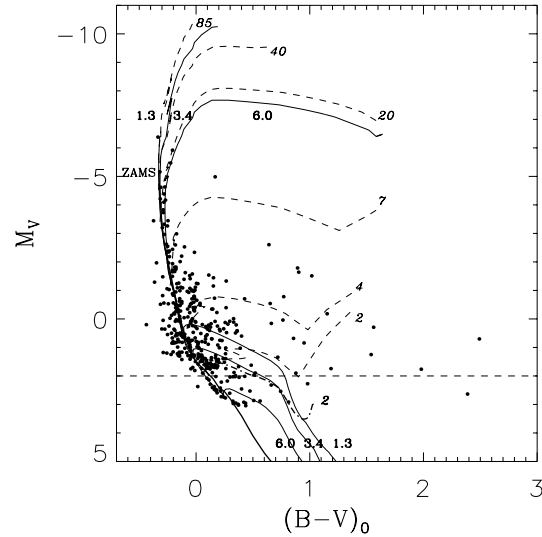


Fig. 10. Color-magnitude diagram of the NGC 6611 members (filled circles). The ZAMS from Schmidt-Kaler (1982) is shown by a thick continuous line. The isochrones for 1.3, 3.4 and 6 Myr are drawn with thin lines labelled with the corresponding ages (bold numbers). Several Post-MS evolutionary tracks are also plotted (dashed lines, numbers in *italics*) and labelled with the corresponding model masses (in solar units). The dotted-dashed line at the bottom labelled with bold italics 2 is the Pre-MS track of $2m_\odot$. The horizontal dashed line is the completeness limit of the sample.

equacy of stellar models, and therefore, should be regarded as a lower limit for the mean errors of the derived parameters.

In addition to the IMF parameters which are traditionally deduced from the LF, we were also able to infer a set of descriptors of the star formation history ($t_0, t_1, \langle t \rangle$) in the cluster. These evolutionary parameters can be derived for young clusters from the comparison of their observed and theoretical LFs provided that an age-dependent detail (H-feature) can be identified in the cluster LF (Piskunov & Belikov 1996). The feature occurs due to the presence of pre-MS stars in young clusters and was found both in the luminosity functions published in the literature (Belikov & Piskunov 1997) and in the Pleiades LF already studied by the authors (Belikov et al. 1998, 1999a).

According to Fig. 9, the observed LF based on the *restricted* sample is affected by the variable absorption at $M_V > 0^m$ and is insufficiently deep to describe completely the H-feature occurring in the theoretical LF ($\phi(M_V)$) at $M_V = 1^m$. In contrast, the observed LF from the *full* sample is in agreement with the “true” theoretical LF down to $M_V = 2^m$. This can be considered as an evidence of the completeness of the *full* sample down to $M_V = 2^m$. We can conclude that the theoretical calibration for the derived cluster parameters is confirmed by the observations and that a significant decrease of the corresponding observed LF at $M_V = 1^m$ is related to the fine structure of the LF and is not caused by an incompleteness of the data. However, the limit of the CC is not sufficient to outline the H-feature completely. This will require much deeper observations.

From the results given in Table 3, the LF analysis provides a reasonable age of cluster stars which is in good agreement

both with independent estimates (from 2 to 6 Myr) by Sagar et al. (1986), Hillenbrand et al. (1993), Massey et al. (1995), De Winter et al. (1997) and with our CMD analysis described below. Also, a considerable age spread among the cluster stars (up to 5 - 6 Myr) derived by Massey et al. (1995) and De Winter et al. (1997) could be confirmed by our results, whereas Hillenbrand et al. (1993) found an age of 1 - 2 Myr for the bulk of their stars (both MS and Pre-MS).

Let us now consider the IMF parameters derived from the LF fit. The slope Γ of the log-normal mass function i.e. the logarithmic derivative of the IMF could be calculated as

$$\Gamma = \frac{d \log f}{d \log m} = -(a + 2b \log m) \log e.$$

The power-law approximation gives the IMF slope $-x = -1.2$ which is common for the whole mass range under study and comparable with $\Gamma = -1.18$ for the log-normal IMF at $m = 10 m_{\odot}$. According to Table 3, the parameter b of a log-normal IMF has a value at the level of its accuracy. Therefore, we may conclude that a power-law approximation (i.e., the case $b = 0$) is sufficient to represent the mass function of NGC 6611 within the studied mass range. The results can be directly compared with the IMF slopes published for NGC 6611.

During the last decade, the mass spectra of NGC 6611 stars have been studied by several authors. Due to the large distance of the cluster, the investigations were mainly restricted to massive stars. Analysing homogeneous photoelectric UBV data and proper motion membership, Sagar et al. (1986) constructed a mass spectrum of a few tens of cluster stars located in the cluster core. The masses were estimated with respect to the theoretical tracks. Within the range $[8.8, 71] m_{\odot}$, the IMF slope was found to be -0.87 ± 0.2 if no mass loss was taken into account, and -0.80 ± 0.3 in the case of a moderate mass loss. Hillenbrand et al. (1993) used optical CCD photometry and spectroscopic data for the construction of IMF in NGC 6611. The masses were also derived with respect to the theoretical tracks. The slope of the IMF was determined for stars with masses above $9 m_{\odot}$ (44 stars) where the mass function could be considered as complete and well defined. The slope was derived to be -1.3 ± 0.2 for all 44 stars and -1.1 ± 0.3 for a sample of stars with the best photometric data. However, re-reducing the same data by using another mass calibration, different theoretical models as well as different scales of effective temperature and bolometric correction, Massey et al. (1995) derived a slope of -0.7 ± 0.2 in a mass range of $[7, 75] m_{\odot}$. This result is similar to the value by Sagar et al. (1986) but differs considerably from the IMF slope suggested for field stars.

In contrast to the published results, we can support our conclusions with about one order of magnitude larger sample of cluster stars. Further, we could extend the investigations to a larger mass range and involve both MS- and PMS models. The slope we derived for IMF of the NGC 6611 cluster is steeper than that by Sagar et al. (1986) and Massey et al. (1995) but it confirms the results by Hillenbrand et al. (1993) and is comparable with the slope found by Scalo (1998) for the IMF of field stars.

Now let us discuss whether our conclusions on the star formation history (e.g., cluster age and age spread) drawn from the LF analysis can be supported by the cluster CMD. In Fig. 10 the $M_V, (B - V)_0$ diagram of NGC 6611 is plotted with superimposed isochrones for the corresponding ages (see Table 3). In order to get an idea on the stellar mass scale, Post-MS tracks are also plotted.

From Fig. 10, a considerable age spread can be concluded among the cluster stars. The t_0 and t_1 isochrones embrace the cluster stars, both around the turn-off point as well as in the vicinity of the turn-on point near $M_V \approx 1^m$. Although a fainter Pre-MS branch is not clearly outlined due to increasing incompleteness below $M_V \approx 2^m$, there is a considerable population of stars located above the main sequence in a wide range of absolute magnitudes ($M_V = -2.0^m \div 3^m$). These objects could be either stars with underestimated reddening or Pre-MS stars still contracting to the main sequence. In the last case, we should suggest a considerable (of order of several Myr) age spread in NGC 6611 and an existence of massive ($m \approx 7 m_{\odot}$) Pre-MS stars at $M_V \approx 0^m$ in the cluster. This statement is in agreement with Sagar et al. (1986), Hillenbrand et al. (1993), and de Winter et al. (1997) who also proposed a presence of massive Pre-MS stars in the cluster. In contrast to Hillenbrand et al. (1993) who found that a typical age of cluster stars is about 1 - 2 Myr, we believe that the cluster stars display the ages within the whole range $[t_0, t_1]$. The question whether this spread results from local effects in star formation history which is probably different in different regions of the cluster or, on the other hand, the star formation history is uniform over the cluster needs an additional careful investigation and is proposed for a future study.

According to the CMD (Fig. 10), a sequential formation of cluster stars is not evident from the present data. Both the most massive MS stars and the Pre-MS stars demonstrate the whole range of ages from t_0 to t_1 .

6. Summary and conclusions

This study was aiming at the construction of the luminosity function and color-magnitude diagram of the young open cluster NGC 6611 and at the analysis of their relation to the star formation history and, especially, to the cluster mass function and age spread in this star-, gas- and dust aggregate.

From the proper motion and photometric data of the Compiled Catalogue published in Paper I, we selected members of NGC 6611 down to $M_V \approx 3^m$ taking into account its general structure and very irregular distribution of absorption across the cluster. This sample is about one order of magnitude larger than the samples previously studied. The observed and theoretical luminosity functions were constructed and compared by taking into account incompleteness of the data at faint magnitudes due to variable absorption. Both log-normal and power-law IMFs were tested and an arbitrary spread of stellar ages in the cluster (at a constant star formation rate) was allowed.

The comparison of the observed and theoretical luminosity functions led us to the following conclusions supported by the analysis of the cluster color-magnitude diagram:

- a. The obtained data allow to find out the H-maximum of the cluster LF, i.e. a feature in the LF structure which is related to the turn-on point of the cluster CMD and can be used as an independent age indicator of the cluster.
- b. Within the studied mass range $m = [2.1, 85] m_{\odot}$, the power-law IMF is sufficient to represent the mass function of the cluster. A slope of $\Gamma = -1.2$ determined for the mass function of NGC 6611 is in good agreement with the slope assumed for the IMF of field stars.
- c. The cluster age of 6 Myr derived both from the LF and CMD analysis is compatible with previous estimations. We also confirm a considerable (of the order of the cluster age) spread of individual ages of cluster stars. No evidence of sequential star formation was found from our data.

Acknowledgements. This research was partly supported by the Deutsche Forschungsgemeinschaft. We thank also the anonymous referee for useful comments and suggestions which helped us to improve the clarity of the paper.

References

- Belikov A.N., Piskunov A.E., 1997, AZh 74, 34
 Belikov A.N., Hirte S., Meusinger H., Piskunov A.E., Schilbach E., 1998, A&A 332, 575
 Belikov A.N., Piskunov A.E., Schilbach E., 1999a, Astron. Nachr. 320, 27
 Belikov A.N., Kharchenko N.V., Piskunov A.E., Schilbach E., 1999b, A&AS 134, 525 (Paper I)
 Hillenbrand L.A., Massey P., Strom S.E., Merrill K.M., 1993, AJ 106, 1906
 Kamp L.W., 1974, A&AS 16, 1
 Massey P., Johnson K.E., DeGioia-Eastwood K., 1995, ApJ 454, 151
 Palla F., Stahler S.W., 1993, ApJ 418, 414
 Piskunov A.E., Belikov A.N., 1996, Pis'ma AZh 22, 522
 Sagar R., Joshi U.C., 1979, A&AS 66, 3
 Sagar R., Piskunov A.E., Myakutin V.I., Joshi U.C., 1986, MNRAS 220, 383
 Scalo, J.M., 1998, In: Gilmore G., Howell D. (eds.) Stellar initial mass function. ASP Conf. Ser. 142, p. 201
 Schaller G., Schaerer D., Meynet G., Maeder A., 1992, A&AS 96, 269
 Schmidt-Kaler Th., 1982, Landolt-Berstein Numerical Data and Functional Relationships in Science and Technology. New Series, Group IV, Springer-Verlag Press, Berlin-Heidelberg, New York, 2, 15
 Silverman B.W., 1986, Density Estimation for Statistics and Data Analysis. Chapman & Hall, London
 Thé P.S., de Winter D., Feinstein A., Westerlund B.E., 1990, A&AS 82, 319
 Tucholke H.-J., Geffert M., Thé P.S., 1986, A&AS 66, 311
 Van Schewick H., 1962, Veröff. Univ. Sternw. Bonn 62, 1
 Walker M.F., 1961, ApJ 133, 438
 de Winter D., Koulis C., Thé P.S., et al., 1997, A&AS 121, 223